JACS
JOURNAL OF THE AMERICAN CHEMICAL SOCIETY

Article

pubs.acs.org/JACS

Electrochemically Induced Chemically Reversible Proton-Coupled Electron Transfer Reactions of Riboflavin (Vitamin B_2)

Serena L. J. Tan and Richard D. Webster*

Division of Chemistry and Biological Chemistry, School of Physical and Mathematical Sciences, Nanyang Technological University, Singapore 637371

Supporting Information

ABSTRACT: The electrochemical behavior of the naturally occurring vitamin B_2, riboflavin (Fl_{ox}), was examined in detail in dimethyl sulfoxide solutions using variable scan rate cyclic voltammetry (ν = 0.1 − 20 V s^{-1}) and has been found to undergo a series of proton-coupled electron transfer reactions. At a scan rate of 0.1 V s^{-1}, riboflavin is initially reduced by one electron to form the radical anion ($Fl_{rad}^{\bullet-}$) at E^0_f = −1.22 V versus Fc/Fc^+ (E^0_f = formal reduction potential and Fc = ferrocene). $Fl_{rad}^{\bullet-}$ undergoes a homogeneous proton transfer reaction with the starting material (Fl_{ox}) to produce $Fl_{rad}H^{\bullet}$ and Fl_{ox}^{-}, which are both able to undergo further reduction at the electrode surface to form $Fl_{red}H^-$ (E^0_f = −1.05 V vs Fc/Fc^+) and $Fl_{rad}^{\bullet 2-}$ (E^0_f = −1.62 V vs Fc/Fc^+), respectively. At faster voltammetric scan rates, the homogeneous reaction between $Fl_{rad}^{\bullet-}$ and Fl_{ox} begins to be outrun, which leads to the detection of a voltammetric peak at more negative potentials associated with the one-electron reduction of $Fl_{rad}^{\bullet-}$ to form Fl_{red}^{2-} (E^0_f = −1.98 V vs Fc/Fc^+). The variable scan rate voltammetric data were modeled quantitatively using digital simulation techniques based on an interconnecting "scheme of squares" mechanism, which enabled the four formal potentials as well as the equilibrium and rate constants associated with four homogeneous reactions to be determined. Extended time-scale controlled potential electrolysis (t > hours) and spectroscopic (EPR and in situ UV−vis) experiments confirmed that the chemical reactions were completely chemically reversible.

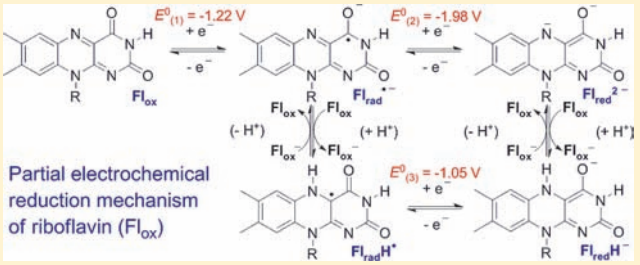

1. INTRODUCTION

Proton-coupled electron transfer (PCET) reactions are of fundamental importance in many chemical and biological processes, including enzymatic and photosynthesis reactions.[1−5] Recently, a number of PCET reactions (especially involving phenols) have been examined in considerable detail, and examples have been reported which occur via concerted (where the electron and proton transfer simultaneously),[6−16] and via consecutive (where the electron and proton transfer separately)[17−19] mechanisms. In this paper, the electrochemical and kinetic parameters associated with a series of chemically reversible proton-coupled electron transfers of a biological molecule have been evaluated, where the proton transfers occur between the neutral starting material and its reduced forms.

Flavin adenine dinucleotide (FAD) and flavin mononucleotide (FMN) are cofactors of enzymes which catalyze many redox reactions in biological systems because of their ability to accept electron pairs from a wide variety of functional groups. These redox reactions include the dehydrogenation of NADPH and D-amino acids.[20−24] Flavoenzymes mediate electron transfer processes in membranes, and are more versatile than nicotinamide coenzymes (NAD and NADP) because they can involve either one- or two-electrons, while nicotinamides can only undergo two-electron processes. This unique versatility allows flavins to act as intermediaries between compounds that donate two electrons (e.g., NADH, succinate) and compounds that only accept one electron at a time (e.g., heme Fe).[20−24] Their unique reactivity with oxygen also enables flavins to take part in important aerobic processes.[20] Riboflavin (Scheme 1) is the primary redox active component of FAD and FMN.

Scheme 1. Riboflavin (Vitamin B_2)

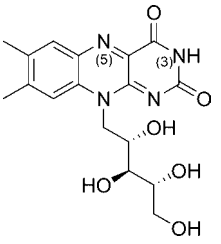

Flavins are comparable to quinones which typically possess three oxidation states: the fully oxidized flavoquinone (Fl_{ox}), the flavosemiquinone radical ($Fl_{rad}^{\bullet-}$), and the two-electron-reduced flavohydroquinone (Fl_{red}^{2-}), each with 3 states of protonation (Scheme 2). The redox properties of flavins in aqueous and protic organic media have been studied previously and it is well-known that in such conditions, the fully oxidized flavoquinone (Fl_{ox}) is immediately reduced to flavohydroquinone ($Fl_{red}H_2$) in

Received: January 7, 2012
Published: March 5, 2012

   dx.doi.org/10.1021/ja300191u | J. Am. Chem. Soc. 2012, 134, 5954−5964

Scheme 2. Possible Flavin Species in Aqueous and Protic Solvents

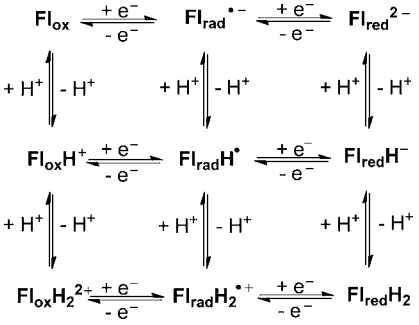

a two-electron and two-proton process.[25−34] While this is useful for modeling systems of flavoenzymes (e.g., assimilatory nitrate reductase,[35] microsomal NADH-cytochrome b_5 reductase[36]) that catalyze two-electron processes, it is not relevant for those flavoenzymes (e.g., flavodoxin[37,38]) that operate via the flavosemiquinone radical. Therefore, an aprotic organic environment is more suitable to model the one-electron processes. Riboflavin is poorly soluble in most solvents suitable for electrochemistry, except for dimethyl sulfoxide where it is soluble up to approximately 4 mM.

This study has investigated the electrochemical reduction of riboflavin in DMSO without an additional proton source, in order to obtain information with respect to the long-term chemical reversibility of the reduction process and to determine whether the starting material can also act as a proton donor. There are several compounds such as the dianion (Fl_{red}^{2-}) and the deprotonated starting material (Fl_{ox}^{-}) that should be detectable by voltammetry if they are formed, but to date have not been reported. The individual species responsible for the voltammetric peaks detected during the forward and reverse scans were identified via variable scan rate CV experiments over a range of concentrations, and by spectroscopic monitoring of the reduction processes via EPR and UV−vis spectroscopies. The detailed voltammetric mechanism that involves a series of chemically reversible proton-coupled electron transfer reactions was modeled using digital simulation techniques, enabling the calculation of all of the kinetic and electrochemical parameters.

2. EXPERIMENTAL SECTION

2.1. Chemicals. *n*-Bu_4NPF_6 was prepared by reacting equal molar amounts of a 40% aqueous solution of *n*-Bu_4OH with a 65% aqueous solution of HPF_6, washing the precipitate with hot water, recrystallizing three times from hot ethanol, and then drying under vacuum for 24 h at 140 °C. Solutions for electrochemical experiments were prepared by adding DMSO (Tedia) and the correct concentration of *n*-Bu_4NPF_6 to predried 3 Å molecular sieves (Fluka) (dried under vacuum at 140 °C for 6 h in a Büchi Glass Oven B-585) and leaving the DMSO/electrolyte in a glass vacuum syringe under a nitrogen atmosphere for at least 36 h. Riboflavin was reagent grade and obtained from Alfa Aesar. ^{1}H NMR experiments confirmed that riboflavin exists in its protonated form in DMSO, since an imide peak was detected at 11.34 ppm (see Figure S9 in Supporting Information).

2.2. Electrochemical Procedures. Cyclic voltammetry (CV) experiments were conducted with a computer-controlled Eco Chemie Autolab PGSTAT 100 with an ADC fast scan generator. Working electrodes used were 0.01, 0.02, 0.05, and 1 mm diameter planar Pt disks, used in conjunction with a Pt auxiliary electrode and a silver wire (0.5 M Bu_4NPF_6 in CH_3CN) reference electrode. Accurate potentials were obtained using ferrocene as an internal standard. The electrochemical cells were dried at 110 °C for a least 1 h prior to use. Solutions of riboflavin (1 mM, 0.5 M *n*-Bu_4NPF_6 in DMSO) for voltammetric analysis were deoxygenated by purging with high purity argon gas and all voltammetric experiments were conducted at 22 (±2) °C in a Faraday cage. Karl Fischer coulometric titrations indicated that the analyte solutions contained 25 mM of H_2O when they were added to the electrochemical cell (DMSO is difficult to be kept dry below this level when placed in an electrochemical cell). Digital simulations of the CV data were performed using the DigiElch 6 software package purchased from Gamry Instruments.

Controlled potential electrolysis was performed in a two-compartment electrolysis cell using Pt mesh as the working and auxiliary electrodes and a silver wire as the reference electrode (separated from the working electrode compartment with a glass membrane containing a solution of 0.5 M *n*-Bu_4NPF_6 in CH_3CN).[17]

2.3. Spectroscopic Experiments. In situ electrochemical UV−vis spectra were obtained using an optically semitransparent thin layer electrochemical (OSTLE) cell at 22 (±2) °C and recorded on a Perkin-Elmer Model Lambda 750 UV−vis-NIR spectrophotometer.[17] EPR spectra were obtained by electrolyzing solutions of riboflavin in DMSO at 22 (±2) °C in an electrolysis cell, transferring the electrolyzed solutions under nitrogen to a quartz flat cell, and recording continuous wave X-band spectra with a Bruker ELEXSYS E500 EPR spectrometer.

3. RESULTS AND DISCUSSION

3.1. Previous Experiments. Studies by Tatwawadi et al.[39] and Sawyer et al.[40] on riboflavin in DMSO showed separately the presence of a reduction process on the forward scan and at least two oxidation waves when the scan direction was reversed. For our initial cyclic voltammogram in DMSO (Figure 1a), we

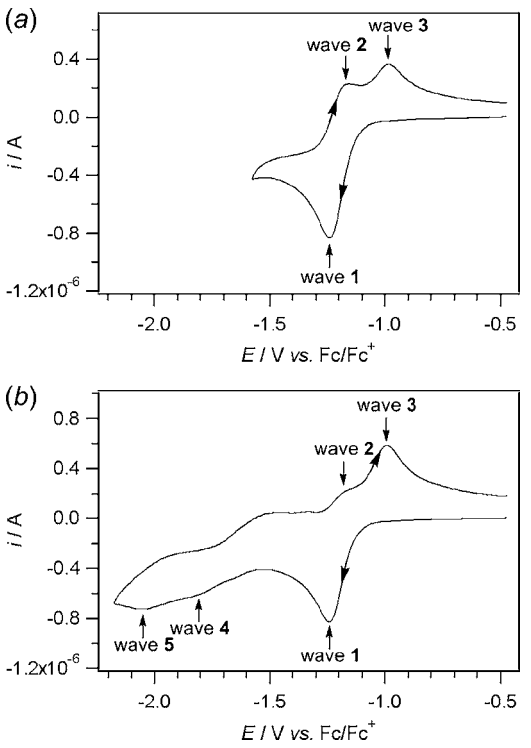

Figure 1. Cyclic voltammograms of the reduction of 1 mM riboflavin at a 1 mm diameter planar Pt electrode in DMSO with 0.5 M *n*-Bu_4NPF_6, and at scan rate 0.1 V s^{-1}. (a) Scan direction reversed at −1.6 V vs Fc/Fc^+. (b) Scan direction reversed at −2.2 V vs Fc/Fc^+.

were also able to observe two oxidation processes (wave **2** and wave **3**) upon reversal of the scan direction after the first reduction process (wave **1**). In the study of riboflavin in DMSO,[39] it was found that wave **2** became larger relative to wave **3** as the

dx.doi.org/10.1021/ja300191u | J. Am. Chem. Soc. 2012, 134, 5954−5964

voltammetric scan rate was increased. Tatwawadi et al.[39] postulated that the species that gave rise to wave **2** was decomposing and so was not observed when the scan rate was too slow. It was also observed that 1 mol of electrons was transferred per mole of riboflavin during bulk electrolysis at potentials held slightly more negative than the first reduction peak potential, and it was concluded that wave **1** corresponds to a single electron transfer, similar to observed for the reduction of quinones in aprotic solvents.[41−45]

Male et al.[34] used EPR spectroscopy to show that a radical species ($Fl_{rad}^{\bullet-}$) was formed by bulk electrolysis at potentials slightly more negative than the first reduction peak potential, and concluded that the radical was formed by comproportionation of the two-electron-reduced Fl_{red}^{2-} and fully oxidized Fl_{ox}, in both water and nonaqueous solvents [proposing that wave **1** involved the initial transfer of two-electrons followed by a comproportionation reaction (eqs 1 and 2)].[34]

$$Fl_{ox} + 2e^- \rightleftharpoons Fl_{red}^{2-} \quad (1)$$

$$Fl_{red}^{2-} + Fl_{ox} \rightleftharpoons 2Fl_{rad}^{\bullet-} \quad (2)$$

Niemz et al.[24] in the most recent study discovered that when the imide proton at N(3) (Scheme 1) was substituted by a methyl group, only wave **2** was observed during the reverse scan (no wave **3**). However, when a proton donor (DH) was added to the solution, two oxidation waves (waves **2** and **3**) could be observed during the reverse scan, with wave **3** being attributed to oxidation of $Fl_{red}H^-$. It was concluded that the initial electron transfer produced the radical anion, $Fl_{rad}^{\bullet-}$ (eq 3) which underwent a rapid intermolecular proton transfer from the proton donor in the bulk solution to form the $Fl_{rad}H^{\bullet}$ radical (eq 4). $Fl_{rad}H^{\bullet}$ was immediately further reduced to $Fl_{red}H^-$ [in either an ECE (eqs 3−5) or DISP1 (eqs 3,4, and 6) mechanism].[46] The oxidation of both $Fl_{rad}^{\bullet-}$ (wave **2**) and $Fl_{red}H^-$ (wave **3**) were proposed to be observed when the scan direction was reversed.[24]

$$Fl_{ox} + e^- \rightleftharpoons Fl_{rad}^{\bullet-} \quad (3)$$

$$Fl_{rad}^{\bullet-} + DH \rightleftharpoons Fl_{rad}H^{\bullet} + D^- \quad (4)$$

$$Fl_{rad}H^{\bullet} + e^- \rightleftharpoons Fl_{red}H^- \quad (5)$$

$$Fl_{rad}^{\bullet-} + Fl_{rad}H^{\bullet} \rightleftharpoons Fl_{red}H^- + Fl_{ox} \quad (6)$$

Bulk electrolysis of N(3)-methylated flavin showed a stronger EPR signal while N(3)-protonated flavin showed a weaker signal and required a longer period of electrolysis.[24] UV−vis spectroelectrochemical experiments were carried out, and the UV spectra of the exhaustively electrolyzed N(3)-protonated species showed that $Fl_{rad}^{\bullet-}$ was formed, and this was attributed to reaction between $Fl_{red}H^-$ and Fl_{ox}^- (Fl_{ox} that has lost a proton) instead of a direct one-electron reduction of Fl_{ox}.

3.2. Cyclic Voltammetry. Figure 2 shows variable scan rate CVs of riboflavin in DMSO, where the current scale has been normalized by multiplying by $\nu^{-0.5}$ (ν = the scan rate in V s^{-1}). It can be observed in Figure 2 that as the scan rate increases, wave **2** becomes larger while concomitantly wave **3** diminishes in magnitude. The change in relative size of waves **2** and **3** can be explained by the reactions in eqs 3−6 (either the ECE or DISP1 mechanisms), where the reduction process (wave **1**) produces the protonated anion ($Fl_{red}H^-$), which can then be voltammetrically oxidized (wave **3**) when the scan direction is reversed. As the scan rate is increased, the protonation reaction of the initially formed radical anion (eq 4) is outrun; hence, wave **2** that is associated with oxidation of the radical anion (the reverse of eq 3) increases in magnitude.

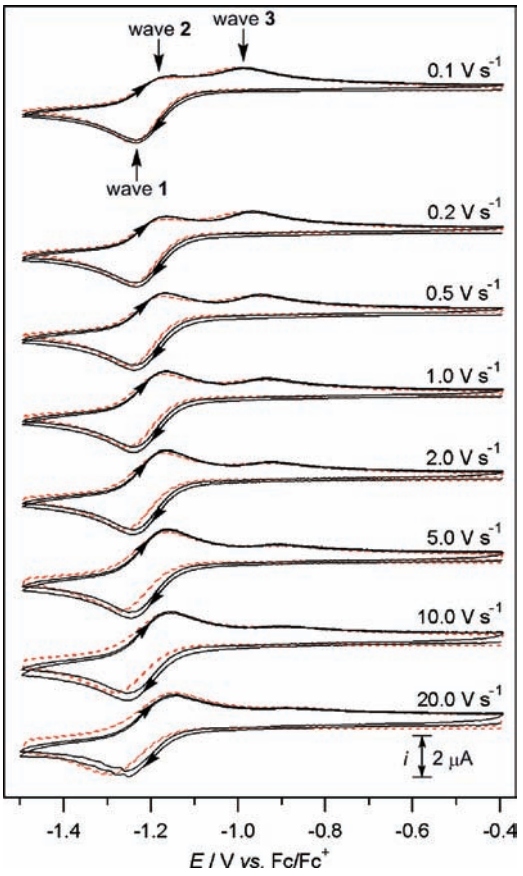

Figure 2. (Black lines) Variable scan rate CVs of 2 consecutive scans of 1 mM riboflavin in DMSO with 0.5 M *n*-Bu_4NPF_6, recorded at a 1 mm Pt electrode at 22 (±2) °C, where the scan direction was reversed at −1.5 V vs Fc/Fc^+. (Red dashed lines) Digital simulations of the CV data based on the mechanism in Scheme 3 and parameters given in Tables 1 and 2. The current data were scaled by multiplying by $\nu^{-0.5}$.

For the experiments in this study, no additional proton donor was added. Therefore, the proton source is likely to be the starting material (Fl_{ox}) which reacts to form the deprotonated anion, Fl_{ox}^- according to eq 7. Controlled potential electrolysis experiments by Tatwawadi et al.[39] in DMSO (and repeated in this present study) confirmed that the overall reaction occurred by one-electron per molecule, which is consistent with half of the Fl_{ox} molecules being reduced by two-electrons and the other half acting as donors of protons (thereby being unavailable for further reduction). Therefore, although wave **1** occurs via two electrons, bulk controlled potential electrolysis of the entire reaction solution occurs via the transfer of only one electron per molecule of starting material. Trace water present in the bulk solution is potentially an alternative source of protons, although in this instance is considered to be an unlikely donor. It was found that the addition of 0.5 M of water to the DMSO did not increase the size of wave **3** relative to wave **2** (at a fixed scan rate) during CV experiments, which supports the hypothesis that water was not acting as a proton donor during the reduction reaction. Furthermore, although DMSO is extremely difficult to dry,[47] it has been shown that the water in DMSO is relatively unreactive

dx.doi.org/10.1021/ja300191u | J. Am. Chem. Soc. 2012, 134, 5954−5964

because it itself undergoes strong hydrogen-bonding with the solvent.[44,45]

$$Fl_{rad}^{\bullet -} + Fl_{ox} \rightleftharpoons Fl_{rad}H^{\bullet} + Fl_{ox}^{-} \quad (7)$$

$$Fl_{rad}^{\bullet -} + e^{-} \rightleftharpoons Fl_{red}^{2-} \quad (8)$$

$$Fl_{red}^{2-} + Fl_{ox} \rightleftharpoons Fl_{red}H^{-} + Fl_{ox}^{-} \quad (9)$$

$$Fl_{ox}^{-} + e^{-} \rightleftharpoons Fl_{rad}^{2-\bullet} \quad (10)$$

Variable scan rate voltammetric experiments were performed at planar electrodes between 10 μm and 1 mm diameter. It was found that at the fastest scan rate (20 V s^{-1}) the anodic (E_p^{ox}) to cathodic (E_p^{red}) peak-to-peak separation (ΔE_{pp}) was similar at the smallest and largest electrode (both were approximately 100 mV). The effects of uncompensated solution resistance are expected to be the highest at the 1 mm electrode and at the fastest scan rate.[48] Therefore, if the ΔE_p-values at the 10 μm and 1 mm diameter electrodes are similar at the higher scan rate of 20 V s^{-1}, the increasing ΔE_{pp}-values shown in Figure 2 with increasing scan rates are due to a relatively slow heterogeneous electron transfer rate (k_s) rather than solely due to uncompensated solution resistance. Experiments performed on ferrocene (where it is assumed that $k_s \geq 1$)[49] under identical conditions showed substantial smaller ΔE_{pp}-values compared to those obtained for riboflavin, supporting a relatively slow rate of heterogeneous electron transfer for riboflavin at a Pt surface in DMSO.

When the scan was extended to more negative potentials, additional reduction waves **4** and **5** were observed at approximately −1.8 and −2.0 V versus Fc/Fc^+, respectively (Figures 1b and 3). Wave **2** was observed to be significantly smaller when the scan direction was reversed just after wave **5** (at −2.2 V vs Fc/Fc^+) compared to when the scan direction was reversed just after wave **1** (at −1.6 V vs Fc/Fc^+) (compare Figures 1a and 1b). In contrast, wave **3** was observed to increase in size if the forward scan direction was extended past wave **5**. Therefore, it is apparent that the electron transfer reactions occurring during wave **5** result in an increase in the amount of species responsible for wave **3**.

It can be observed in Figure 3 that the current magnitude of wave **5** increases as the scan rate increases, while concomitantly wave **4** decreases in current magnitude as the scan rate increases. Therefore, it is proposed that wave **5** is associated with further one-electron reduction of $Fl_{rad}^{\bullet -}$ to form the dianion (Fl_{red}^{2-}) according to eq 8. Fl_{red}^{2-} is then able to rapidly gain a proton (from an intermolecular exchange with Fl_{ox} to form $Fl_{red}H^-$ (eq 9), which can then be oxidized in wave **3** (the reverse of eq 5). The position of wave **5** is consistent with what is often observed during the reduction of semiquinones in nonaqueous solvents, where the second electron transfer step (to form the dianion) occurs several hundred mV more negative than the first electron transfer step (to form the anion radical).[41−45] The assignment of wave **5** as associated with one-electron reduction of $Fl_{rad}^{\bullet -}$ negates the possibility that wave **1** occurs via a direct two-electron reduction to form the dianion (eq 1). Because the species responsible for waves **4** and **5** are present at the electrode surface at lower concentrations than the starting material, they are more easily detected by a differential voltammetric scanning technique such as square-wave voltammetry (see Figure S8 in the Supporting Information).

Wave **4** is only noticeable at slow scan rates (ν < ~2 V s^{-1}) and can be observed to decrease in magnitude proportionally to

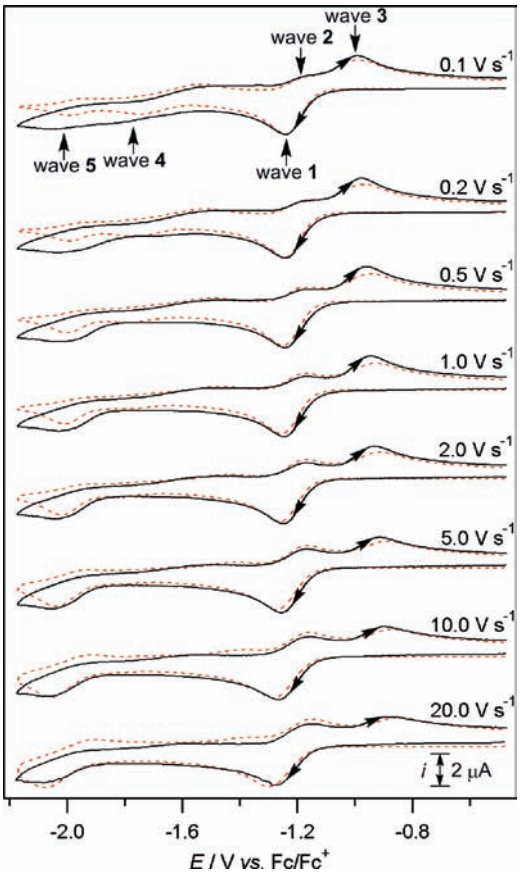

Figure 3. (Black lines) Variable scan rate CVs of 1 mM riboflavin in DMSO with 0.5 M *n*-Bu_4NPF_6, recorded at a 1 mm Pt electrode at 22 (±2) °C, where the scan direction was reversed at −2.2 V vs Fc/Fc^+. (Red dotted lines) Digital simulations of the CV data based on the mechanism in Scheme 3 and parameters given in Tables 1 and 2. The current data were scaled by multiplying by $\nu^{-0.5}$.

wave **2** increasing in magnitude as the scan rate is increased. As the scan rate increases, the reaction between Fl_{ox} and $Fl_{rad}^{\bullet -}$ is outrun (eq 7); hence, it would be expected that the amount of Fl_{ox}^- at the electrode surface would also diminish. Therefore, wave **4** has been assigned as due to the reduction of Fl_{ox}^- (eq 10), which would be expected to be harder to reduce than the neutral starting material (Fl_{ox}) due to its increased negative charge. The peak current of wave **4** is slightly smaller than expected and the voltammetric wave drawn out over a wide potential range, which can be accounted for by the process involving relatively slow heterogeneous electron transfer.

To show that wave **4** is indeed associated with the reduction of Fl_{ox}^-, 1 equiv of the strong base *n*-Bu_4NOH (40% in water) was added to a solution of 1.5 mM riboflavin, turning the bright yellow colored solution into a dark brown colored solution. The resulting product was analyzed via cyclic voltammetry and it was found that wave **1** had disappeared, showing that Fl_{ox} had been successfully deprotonated to form Fl_{ox}^-, while wave **4** increased significantly (Figure 4). Wave **4** in Figure 4 appears larger when the Fl_{ox}^- is produced via reaction with base (dotted blue line) rather than when formed via eq 7 (black line). This is because, in the absence of base, Fl_{ox}^- undergoes other homogeneous reactions and is thus partially removed from the vicinity of the electrode surface.

3.3. Controlled Potential Electrolysis. Bulk controlled potential electrolysis and coulometry experiments were

dx.doi.org/10.1021/ja300191u | J. Am. Chem. Soc. 2012, 134, 5954−5964

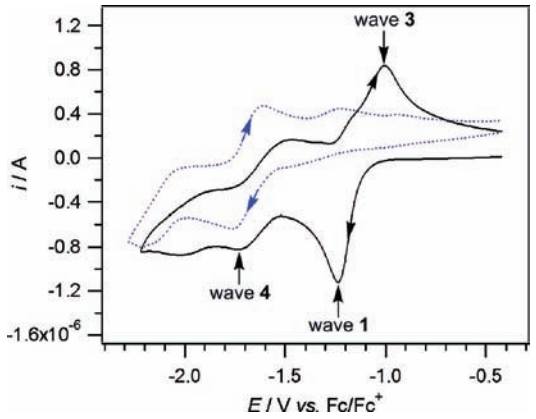

Figure 4. Cyclic voltammograms of 1.5 mM riboflavin in DMSO with 0.5 M *n*-Bu_4NPF_6, recorded at a 1 mm Pt electrode at 22 (±2) °C and at a scan rate of 0.1 V s^{-1}: (black line) before addition of *n*-Bu_4NOH; (dotted blue line) after addition of *n*-Bu_4NOH.

performed in order to determine the number of electrons transferred and to estimate the lifetime of the reduced compounds. The applied potential was set at approximately −1.0 V versus Ag wire (separated from the test solution with a salt bridge containing 0.5 M *n*-Bu_4NPF_6 in CH_3CN), which was approximately −0.2 V more negative than the reduction peak (E_p^{red}). During the electrolysis, the solution color was observed to change from yellow to reddish-brown. The black solid line in Figure 5a is the CV obtained in the working electrode compartment of the electrolysis cell (at a 1 mm diameter Pt electrode) prior to the electrolysis and the blue dotted line is the CV obtained at the completion of the electrolysis. It is significant to observe that the position of zero current in the voltammograms in Figure 5a shift between the start (black solid line) and finish of the electrolysis (blue dotted line), and indicates that the reduced compound exists in a charged state, and can undergo oxidation by applying a potential more positive than approximately −0.6 V versus Ag wire (0.5 M *n*-Bu_4NPF_6 in CH_3CN).

The data in Figure 5b are the current versus time trace obtained during the electrolysis (black solid line) and the corresponding charge (the integrated current vs time) that has been converted into electrons transferred per molecule (red dotted line). The coulometry data confirm that close to one electron per molecule (0.95) is transferred during the reduction step. At the completion of the electrolysis, an oxidizing potential of approximately −0.5 V versus Ag wire (0.5 M *n*-Bu_4NPF_6 in CH_3CN) was applied to the working electrode, which resulted in the transfer of 0.85 electrons per molecule and the regeneration of the starting material. We have previously observed that the reverse electrolysis step does not always quantitatively regenerate the starting material (even if the reduced species is indefinitely long-lived) because some of the reduced product may diffuse into the other compartment of the electrolysis cell and so may be lost.[17] The resultant CV obtained at the completion of the reverse electrolysis reaction was identical to the CV of riboflavin and the color of the solution turned from reddish-brown back to yellow, indicating that riboflavin is recovered upon oxidation on electrolysis time scales (hours) and confirming that its reduced forms are long-lived in DMSO solution.

3.4. UV−Vis and EPR Experiments. To spectroscopically confirm that the reduced compounds ($Fl_{rad}^{\bullet-}$ and $Fl_{red}H^-$)

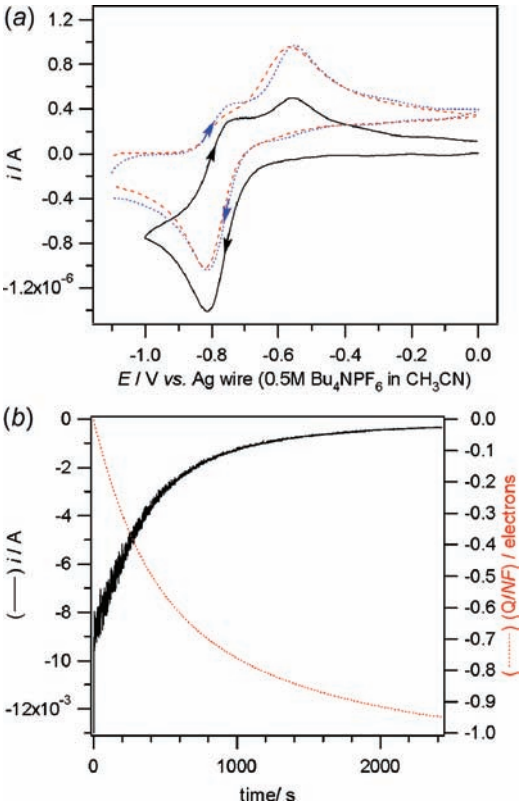

Figure 5. Voltammetric and coulometric data obtained at 22 (±2) °C during the controlled potential electrolysis of 2 mM riboflavin in DMSO with 0.5 M *n*-Bu_4NPF_6. (a) Cyclic voltammograms recorded at a scan rate of 0.1 V s^{-1} with a 1 mm diameter planar Pt electrode: (black line) before the bulk reduction of riboflavin; (blue dotted line) after the exhaustive reduction of riboflavin; (red dashed line) simulated voltammogram according to the reaction in Scheme 3 and parameters in Tables 1 and 2. (b) Current/coulometry vs time data obtained during the exhaustive reduction of riboflavin at −1.0 V vs Ag wire (0.5 M *n*-Bu_4NPF_6 in CH_3CN).

could be oxidized back into riboflavin without forming any other decomposition products, in situ electrochemical UV−vis spectroscopic experiments were performed in an OSTLE cell.[17] Figure 6a shows the spectra obtained during forward reduction reaction, Figure 6b shows the reverse oxidation reaction, and Figure 6c shows the spectra obtained before the electrolysis was commenced (black line), and after the reduced compound had been oxidized back to the starting material (dotted blue line). The data in Figure 6c confirm the complete regeneration of the starting material after electrolysis (the entire experiment was performed over a period of approximately 1 h at 22 ± 2 °C).

During the bulk reduction of riboflavin, the peaks with absorption maxima at 445 nm, 343 and 268 nm were observed to decrease, concomitantly to the growth of peaks with absorption maxima at 257 and 370 nm. The flavosemiquinone radical $Fl_{rad}^{\bullet-}$ has characteristic absorption maxima at around 370 nm and a smaller peak at approximately 478 nm, as shown by Niemz et al.[24] using a modified N-methylated flavin that is able to undergo reduction to obtain purely the radical anion $Fl_{rad}^{\bullet-}$. The modified N-methylated flavin with a proton donor can be reduced into $Fl_{red}H^-$, with only a shoulder absorption around 360 nm.[24] However, in our UV−vis spectra, a shoulder (rather than a clear peak) was observed at 478 nm due to a significant amount of $Fl_{red}H^-$ in solution with $Fl_{rad}^{\bullet-}$. We also

dx.doi.org/10.1021/ja300191u | J. Am. Chem. Soc. 2012, 134, 5954−5964

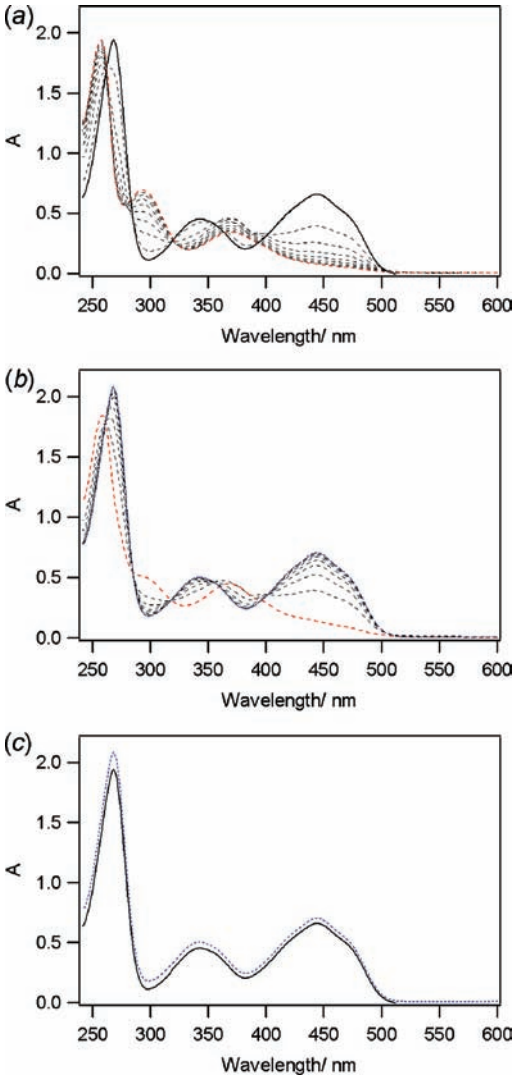

Figure 6. In situ electrochemical UV−vis spectra of 1 mM riboflavin in DMSO containing 0.5 M n-Bu_4NPF_6. (a) Obtained during the reduction of riboflavin; (b) obtained during the reoxidation of the reduced forms of riboflavin ($Fl_{rad}^{\bullet-}$ and $Fl_{red}H^-$); (c) A comparison of (black line) riboflavin and (dotted blue line) after the reduced compound had been oxidized back to the starting material.

did not observe a bright red color after electrolysis, but a dull reddish-brown, likely to be a mixture of the red $Fl_{rad}^{\bullet-}$ and the dull yellow $Fl_{red}H^-$.

EPR experiments were performed by electrochemically reducing solutions of riboflavin in DMSO in an electrolysis cell and transferring an aliquot of the electrolysis solution into a silica flat cell under a nitrogen atmosphere. A radical signal was detected (Figure 7a) with a g-value of 2.0048 whose spectrum is the same as has been previously observed during the reduction of riboflavin in DMSO.[34] The EPR signal showed no change in intensity over a period of at least 3 h, indicating that the detected radical was long-lived. The CV and electrolysis experiments conducted on Fl_{ox} indicate that the major product of the electrochemical reduction is not $Fl_{rad}^{\bullet-}$; otherwise, wave **2** would clearly be evident during slow scan rate CV experiments (Figures 1−3) and when a CV is conducted at the completion of controlled potential electrolysis (Figure 5). Instead the major product of the electrolysis experiments is the diamagnetic $Fl_{red}H^-$. Therefore, the detection of a long-lived

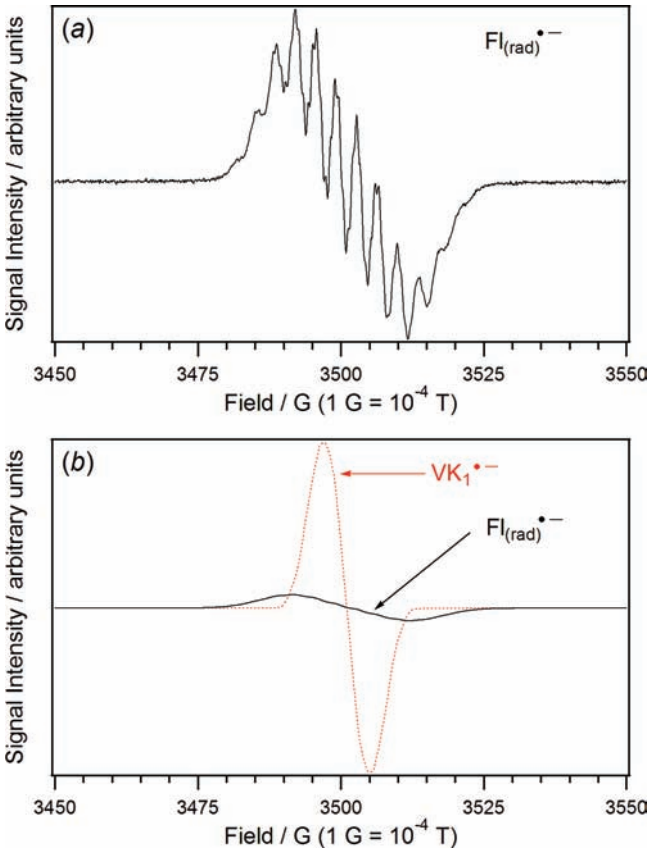

Figure 7. (a) Continuous wave X-band EPR spectrum of a 2 mM solution of riboflavin that had been exhaustively reduced in DMSO containing 0.5 M n-Bu_4NPF_6 via controlled potential electrolysis by one-electron per molecule to partially form [$Fl_{rad}^{\bullet-}$] according to Scheme 3. Modulation amplitude = 0.2 G, T = 22 (±2) °C. (b) Continuous wave X-band EPR spectra of separate solutions of 2 mM riboflavin and 2 mM vitamin K_1 in DMSO containing 0.5 M n-Bu_4NPF_6 that had been exhaustively reduced via controlled potential electrolysis by one-electron per molecule to form $Fl_{rad}^{\bullet-}$ (plus $Fl_{red}H^-$) and $VK_1^{\bullet-}$, respectively. Modulation amplitude = 10 G, T = 22 (±2) °C.

radical can be accounted for by an equilibrium between $Fl_{red}H^-$ and Fl_{ox}^- to produce 2 molecules of $Fl_{rad}^{\bullet-}$ (eq 11).

$$Fl_{red}H^- + Fl_{ox}^- \rightleftharpoons 2Fl_{rad}^{\bullet-} \quad (11)$$

Provided that the equilibrium constant in eq 11 is low, $Fl_{rad}^{\bullet-}$ will appear to exist as a long-lived radical, albeit with a lower EPR signal intensity than expected for the major product. Quantitative EPR experiments were conducted by over-modulating the EPR signal obtained during the electrolysis of Fl_{ox} and comparing the signal intensity with the long-lived radical anion produced during the one-electron reduction of vitamin K_1 (VK_1),[44] under identical instrumental and experimental condition. Figure 7b shows that the radical anion signal of reduced vitamin K_1($VK_1^{\bullet-}$) is significantly more intense than that of $Fl_{rad}^{\bullet-}$, which supports the assignment of the radical anion produced during the reduction of Fl_{ox} as a product formed by a secondary equilibrium process (eq 11). The integrated EPR absorption spectrum of $Fl_{rad}^{\bullet-}$ was found to be 40% of the integrated signal intensity of $VK_1^{\bullet-}$, with the two solutions produced by electrolysis and the EPR spectra recorded under identical instrumental conditions.

3.5. Digital Simulation of CV Data. There are a number of reports of both organic and inorganic compounds that

dx.doi.org/10.1021/ja300191u | J. Am. Chem. Soc. 2012, 134, 5954−5964

Scheme 3. Voltammetrically Induced Proton-Coupled Electron Transfer Reduction Mechanism of Riboflavin in DMSO Studied by Cyclic Voltammetry over a Range of Scan Rates and Concentrations[a]

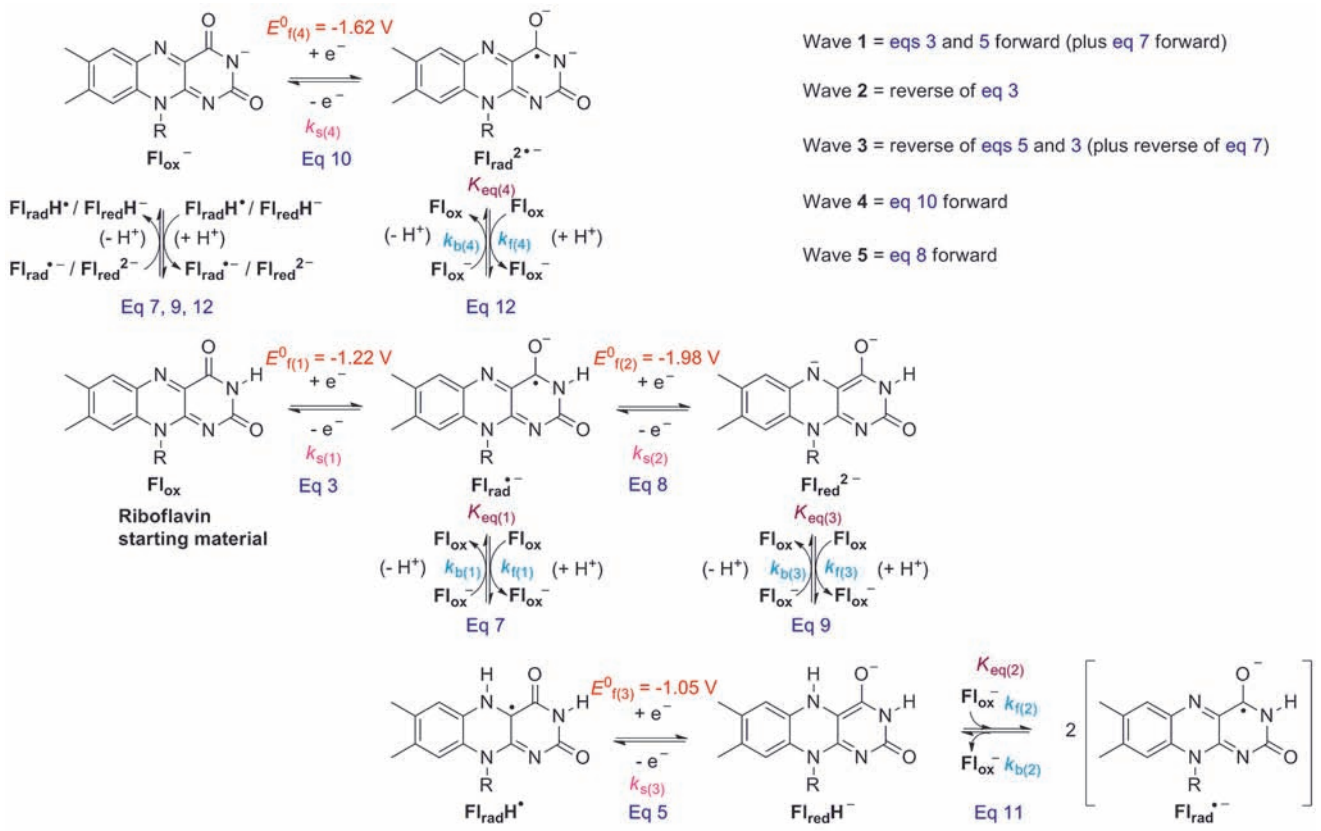

[a]Electrochemical, equilibrium and kinetic values associated with the heterogeneous electron transfer steps ($E^0_{f(1)} - E^0_{f(4)}$) (eqs 3, 5, 8, and 10) and homogeneous chemical steps (eqs 7, 9, 11, and 12) are given in Tables 1 and 2. Only one resonance structure is given for each compound and the counterions for the charged species are either the supporting electrolyte cation (n-Bu_4N^+) or anion (PF_6^-).

undergo reversible structural changes (such as ligand substitutions about a metal ion or proton transfer reactions) prior to, during, or after the electron transfer steps. When the electron transfer steps and reversible chemical transformations occur in a consecutive fashion, the square-scheme mechanism results.[50−62] The complete electrochemical reduction mechanism of riboflavin in DMSO is given in Scheme 3, based on the electrochemical and spectroscopic experiments, which comprises a number of square schemes involving proton transfer and electron transfer reactions. It is known that the presence of the imide proton on N(3) (or the addition of a proton source) is critical to the observation of wave **3**;[24] hence, the proton must be involved in the coupled chemical reactions. Therefore, the proposed reactions are based on intermolecular proton transfer of the imide proton of the starting material Fl_{ox} to the nitrogen atom on other reduced riboflavin molecules as shown diagrammatically in Scheme 3.

For slow scan rates and a low switching potential of −1.6 V versus Fc/Fc^+, riboflavin (Fl_{ox}) is first reduced by one electron to $Fl_{rad}^{\bullet-}$ ($E^0_{f(1)}$), which receives a proton from another Fl_{ox} molecule to form $Fl_{rad}H^{\bullet}$ and the deprotonated Fl_{ox} (Fl_{ox}^-) (eq 7). Since the $E^0_{f(3)}$ (−1.05 V vs Fc/Fc^+) for the reduction of $Fl_{rad}H^{\bullet}$ to $Fl_{red}H^-$ is less negative than the $E^0_{f(1)}$ (−1.22 V vs Fc/Fc^+) for the reduction of Fl_{ox} to $Fl_{rad}^{\bullet-}$, $Fl_{rad}H^{\bullet}$ will be instantly reduced at the electrode surface to $Fl_{red}H^-$ (or can react via a disproportionation reaction according to eq 6). The Fl_{ox}^- and $Fl_{red}H^-$ species can also undergo a comproportionation reaction (involving an electron and proton exchange) to form two molecules of $Fl_{rad}^{\bullet-}$ (eq 11). Because of the K_{eq} of the comproportionation reaction in eq 11 being <1, the majority of the $Fl_{red}H^-$ remains in solution and is detected during the reverse oxidation scan (wave **3**). At fast scan rates, the rate constant of the proton transfer step (eq 7) is outrun and wave **2** is observed due to the one-electron oxidation of $Fl_{rad}^{\bullet-}$ back to Fl_{ox}.

For slow scan rates and a more negative switching potential of −2.2 V versus Fc/Fc^+, two additional reduction waves are observed (waves **4** and **5**). Wave **4** is associated with the reduction of Fl_{ox}^- ($E^0_{f(4)}$) and wave **5** is due to the reduction of $Fl_{rad}^{\bullet-}$ ($E^0_{f(2)}$). As the scan rate increases, wave **4** becomes smaller (because there is less time for Fl_{ox}^- to be produced according to the reaction between $Fl_{rad}^{\bullet-}$ and Fl_{ox}), while wave **5** becomes larger (as there is more $Fl_{rad}^{\bullet-}$ able to undergo further reduction). Fl_{red}^{2-} can convert into $Fl_{red}H^-$ according to eq 9. $Fl_{rad}^{\bullet-}$ is in equilibrium with $Fl_{rad}^{2\bullet-}$ according to eq 12, and the deprotonation of Fl_{ox} (shown on the left of Scheme 3) can occur via eqs 7, 9, and 12.

$$Fl_{rad}^{2-\bullet} + Fl_{ox} \rightleftharpoons Fl_{rad}^{\bullet-} + Fl_{ox}^- \quad (12)$$

Digital simulations were performed on the cyclic voltammetric data that were obtained at scan rates between 0.1 and 20 V s^{-1}, for concentrations of riboflavin between 1 and 3.6 mM, and at a Pt working electrode with a diameter of 1 mm. The data were modeled according to the entire mechanism in Scheme 3 with the electrochemical and kinetic parameters

dx.doi.org/10.1021/ja300191u | J. Am. Chem. Soc. 2012, 134, 5954−5964

Table 1. Electrochemical Parameters Obtained by Digital Simulation of CV[a] Data for the Reaction Mechanism Given in Scheme 3

		$Fl_{ox} + e^- \rightleftharpoons Fl_{rad}^{\bullet -}$ (Eq 3)		$Fl_{rad}^{\bullet -} + e^- \rightleftharpoons Fl_{red}^{2-}$ (Eq 8)		$Fl_{radH}^{\bullet} + e^- \rightleftharpoons Fl_{red}H^-$ (Eq 5)		$Fl_{ox}^- + e^- \rightleftharpoons Fl_{rad}^{2-\bullet}$ (Eq 10)	
D/cm^2 s^{-1}	R/Ω	$E^0_{(1)}$[b]/V	$k_{s(1)}$/ cm s^{-1}	$E^0_{(2)}$[b]/V	$k_{s(2)}$/cm s^{-1}	$E^0_{(3)}$[b]/V	$k_{s(3)}$/cm s^{-1}	$E^0_{(4)}$[b]/V	$k_{s(4)}$/cm s^{-1}
1.6×10^{-6}	1000	−1.22	0.02	−1.98	0.01	−1.05	0.001	−1.62	0.0004

[a]CV data recorded in DMSO at 22 (±2) °C with 0.5 M n-Bu_4NPF_6 as the supporting electrolyte with a 1 mm diameter planar Pt working electrode and at scan rates between 0.1 and 20 V s^{-1}. [b]Formal potential vs Fc/Fc$^+$ (add 0.43 V to convert to vs SCE[67]).

Table 2. Equilibrium and Rate Constants Obtained by Digital Simulation of CV Data for the Reaction Mechanism Given in Scheme 3 Obtained in DMSO Containing 0.5 M Bu_4NPF_6 at 22 (±2) °C

$Fl_{rad}^{\bullet -} + Fl_{ox} \rightleftharpoons Fl_{radH}^{\bullet} + Fl_{ox}^-$ (Eq 7)			$Fl_{redH}^- + Fl_{ox}^- \rightleftharpoons 2Fl_{rad}^{\bullet -}$ (Eq 11)			$Fl_{red}^{2-} + Fl_{ox} \rightleftharpoons Fl_{redH}^- + Fl_{ox}^-$ (Eq 9)			$Fl_{rad}^{2-\bullet} + Fl_{ox} \rightleftharpoons Fl_{rad}^{\bullet -} + Fl_{ox}^-$ (Eq 12)		
$K_{eq(1)}$	$k_{f(1)}$/L mol^{-1} s^{-1}	$k_{b(1)}$/L mol^{-1} s^{-1}	$K_{eq(2)}$	$k_{f(2)}$/L mol^{-1} s^{-1}	$k_{b(2)}$/L mol^{-1} s^{-1}	$K_{eq(3)}$	$k_{f(3)}$/L mol^{-1} s^{-1}	$k_{b(3)}$/L mol^{-1} s^{-1}	$K_{eq(4)}$	$k_{f(4)}$/L mol^{-1} s^{-1}	$k_{b(4)}$/L mol^{-1} s^{-1}
8.00×10^{-3}	1.00×10^6	1.25×10^8	1.67×10^{-1}	2.00×10^2	1.19×10^3	4.17×10^{13}	$>1.00 \times 10^6$	2.40×10^{-8}	5.76×10^6	1.00×10^4	1.74×10^{-3}

dx.doi.org/10.1021/ja300191u | J. Am. Chem. Soc. 2012, 134, 5954−5964

obtained by the simulations given in Tables 1 and 2, respectively. The simulated voltammograms are given as the dashed red lines in Figures 2, 3, and 5 for 1 mM of riboflavin, with additional simulated voltammograms for different concentrations of riboflavin provided in the Supporting Information. The simulations were based on the ECE (eqs 3−5) mechanism rather than the DISP1 (eqs 3, 4, and 6) mechanism. Because of the large number of steps involved in the reaction, it is very difficult to voltammetrically distinguish between the two possibilities (ECE or DISP1). Furthermore, the electron transfer and homogeneous reactions were all modeled based on consecutive pathways, rather than on concerted pathways, which are also difficult to ascertain due to the large number of homogeneous steps involved.

The simulations use exactly the same electrochemical and kinetic parameters for all of the scan rates and concentrations of riboflavin. A good match between the experimental and simulated voltammograms could be obtained, which supports the assignment of the overall reaction given in Scheme 3. It can also be observed in Figure 5 that the simulation that was obtained from the reduced solution of riboflavin (that contains $Fl_{red}H^-$ and $Fl_{rad}^{\bullet-}$) using the same parameters as given in Tables 1 and 2, also matched the experimentally obtained voltammogram, which supports the overall mechanism.

All the parameters in Tables 1 and 2 were entered into each simulation, although the effects of the different rate and equilibrium constants are not noticeable at all of the scan rates; therefore, the simulations need to match over a range of scan rates in order to obtain the optimal kinetic values. The thermodynamic nature of the square scheme means that the equilibrium constants and formal potentials are interrelated. Thus, if one equilibrium constant (e.g., $K_{eq(1)}$) and two formal potentials (e.g., $E^0_{f(2)}$ and $E^0_{f(3)}$) are known, then the second equilibrium constant in the square scheme (i.e., $K_{eq(3)}$) can be automatically calculated.[63,64]

The estimated formal potentials in Table 1 are given versus the ferrocene$^{0/+}$ redox couple, which is the recommended reference standard for nonaqueous solvents.[65,66] To convert to the saturated calomel electrode (SCE) scale, 0.43 V can be added to the values in Table 1.[66,67] The forward rate constant in eq 9 is the minimum value which allowed a good fit of the simulation to the experimental data, although the true value could approach the diffusion limited maximum ($\sim 1 \times 10^{10}$ L mol^{-1} s^{-1}). The heterogeneous electron transfer rate ($k_{s(4)}$) for eq 10 was estimated to be particularly low; 2 orders of magnitude less than $k_{s(1)}$ for the initial electron transfer step. The Marcus Microscopic model of electron transfer predicts that electron transfer reactions involving large structural changes tend to be slow; thus, the low $k_{s(4)}$-value possibly results from the transformation between Fl_{ox}^- and $Fl_{rad}^{2-\bullet}$ involving a particularly large structural change.[48] Surface/solute interactions may also be important, since it was found that when glassy carbon (GC) rather than Pt was used as the electrode surface, the voltammetric waves became more drawn out, suggesting even slower heterogeneous electron transfer rates.

3.6. Relevance of Electrochemical Results to Proteins with Riboflavin Based Cofactors. In NADH-cytochrome b_5 reductase, the flavin cofactor is located in a large cleft between the two main domains of the protein,[68] and is readily accessible to water molecules, thus is able to undergo a $2e^-/2H^+$ reduction directly to $Fl_{red}H_2$,[69] which is the well-established reduction mechanism for free flavins in aqueous solutions.

In flavodoxin, because the proton at N(3) (Scheme 1) is strongly hydrogen-bonded to the protein,[70] it is unable to act as a proton donor for a second flavin cofactor. Instead, after one-electron reduction, N(5) undergoes protonation by a nearby amide proton of the protein backbone.[71,72] It has been proposed that the reduction potential of the protonated semiquinone ($Fl_{rad}H^{\bullet}$) is more negative than that of $Fl_{rad}H^{\bullet}$ in free FMN by 300−400 mV, due to stabilization of the $Fl_{rad}H^{\bullet}$ by H-bonding interactions of NH(5) with a carbonyl oxygen.[72] Therefore, after $Fl_{rad}^{\bullet-}$ is protonated to form $Fl_{rad}H^{\bullet}$, it is not necessarily immediately further reduced, as occurs in this study. This indicates the importance of the protein structure in stabilizing the different forms of the flavoquinones, and if a slight conformation change or mutation occurs, the electron transfer mechanism may also vary significantly.

Because of the role of a neighboring Fl_{ox} acting as a proton donor to $Fl_{rad}^{\bullet-}$, this study has more significance for flavoenzymes containing two or more flavin molecules, such as hepatic NADPH-cytochrome P-450 reductase and Na^+-pumping NADH-ubiquinone oxidoreductase. For Na^+-pumping NADH-ubiquinone oxidoreductase, which has two covalently bonded FMN molecules, one noncovalently bonded FAD and one noncovalently bonded riboflavin, it has recently been shown that the radical anion ($Fl_{rad}^{\bullet-}$) was present in the fully reduced enzyme,[73,74] a species not detectable in the reduced flavodoxin. It is believed that this study may provide insights on the mechanisms of similar enzymes.

CONCLUSIONS

Bulk controlled potential electrolysis and spectroscopic experiments indicated that the net electrochemical reduction of riboflavin in DMSO occurred by one-electron per molecule and was completely chemically reversible on the hours time scale at 22 (±2) °C, indicating that both the radical anion ($Fl_{rad}^{\bullet-}$) and the further reduced and protonated anion ($Fl_{red}H^-$) were very long-lived. Quantitative EPR experiments led to the estimation that $Fl_{rad}^{\bullet-}$ existed in approximately 40% yield based on the exhaustive electrolysis of the starting material. However, the CV experiments in conjunction with the digital simulations indicated that the persistent existence of $Fl_{rad}^{\bullet-}$ in the bulk solution (produced during controlled potential electrolysis experiments) was a result of the homogeneous reaction between $Fl_{red}H^-$ and Fl_{ox}^- to form 2 $Fl_{rad}^{\bullet-}$ (eq 11) rather than by direct one-electron reduction of Fl_{ox} to form $Fl_{rad}^{\bullet-}$. While the EPR spectroscopic experiments are only sensitive to the existence of radicals, the UV−vis spectrum of the reduced solution represented a mixture of both $Fl_{rad}^{\bullet-}$ and $Fl_{red}H^-$. CV experiments confirmed the existence of Fl_{ox}^- and Fl_{red}^{2-} via the identification of their voltammetric waves, which allowed the assignment of their formal electrode potentials.

ASSOCIATED CONTENT

Supporting Information

Variable scan rate cyclic voltammograms obtained at different sized electrodes (0.01−0.05 mm diameter), variable scan rate cyclic voltammograms and their associated digitally simulated traces obtained at different concentrations of riboflavin (2−3.6 mM), square-wave voltammogram of riboflavin, and ^{1}H NMR spectrum of riboflavin in DMSO-d_6. This material is available free of charge via the Internet at http://pubs.acs.org.

dx.doi.org/10.1021/ja300191u | J. Am. Chem. Soc. 2012, 134, 5954−5964

AUTHOR INFORMATION

Corresponding Author

webster@ntu.edu.sg

Notes

The authors declare no competing financial interest.

ACKNOWLEDGMENTS

This work was supported by a Singapore Government Ministry of Education research grant (T208B1222). S.L.J.T. thanks NTU for the award of a Nanyang President's Graduate Scholarship (NPGS).

REFERENCES

(1) Huynh, M. H. V.; Meyer, T. J. *Chem. Rev.* **2007**, *107*, 5004−5064.
(2) Costentin, C. *Chem. Rev.* **2008**, *108*, 2145−2179.
(3) Costentin, C.; Robert, M.; Savéant, J.-M. *Acc. Chem. Res.* **2010**, *43*, 1019−1029.
(4) Warren, J. J.; Tronic, T. A.; Mayer, J. M. *Chem. Rev.* **2010**, *110*, 6961−7001.
(5) Bonin, J.; Robert, M. *Photochem. Photobiol.* **2011**, *87*, 1190−1203.
(6) Rhile, I. J.; Mayer, J. M. *J. Am. Chem. Soc.* **2004**, *126*, 12718−12719.
(7) Costentin, C.; Robert, M.; Savéant, J.-M. *J. Am. Chem. Soc.* **2006**, *128*, 4552−4553.
(8) Rhile, I. J.; Markle, T. F.; Nagao, H.; DiPasquale, A. G.; Lam, O. P.; Lockwood, M. A.; Rotter, K.; Mayer, J. M. *J. Am. Chem. Soc.* **2006**, *128*, 6075−6088.
(9) Costentin, C.; Robert, M.; Savéant, J.-M. *J. Am. Chem. Soc.* **2006**, *128*, 8726−8727.
(10) Markle, T. F.; Mayer, J. M. *Angew. Chem., Int. Ed.* **2008**, *47*, 738−740.
(11) Costentin, C.; Louault, C.; Robert, M.; Savéant, J.-M. *J. Am. Chem. Soc.* **2008**, *130*, 15817−15819.
(12) Costentin, C.; Louault, C.; Robert, M.; Savéant, J.-M. *Proc. Natl. Acad. Sci. U.S.A.* **2009**, *106*, 18143−18148.
(13) Costentin, C.; Robert, M.; Savéant, J.-M. *Phys. Chem. Chem. Phys.* **2010**, *12*, 11179−11190.
(14) Bonin, J.; Costentin, C.; Louault, C.; Robert, M.; Savéant, J.-M. *J. Am. Chem. Soc.* **2011**, *133*, 6668−6674.
(15) Mayer, J. M. *Acc. Chem. Res.* **2011**, *44*, 36−46.
(16) Bonin, J.; Costentin, C.; Robert, M.; Savéant, J.-M. *Org. Biomol. Chem.* **2011**, *9*, 4064−4069.
(17) Williams, L. L.; Webster, R. D. *J. Am. Chem. Soc.* **2004**, *126*, 12441−12450.
(18) Webster, R. D. *Acc. Chem. Res.* **2007**, *40*, 251−257.
(19) Yao, W. W.; Peng, H. M.; Webster, R. D.; Gill, P. M. W. *J. Phys. Chem. B* **2008**, *112*, 6847−6855.
(20) Walsh, C. *Acc. Chem. Res.* **1980**, *13*, 148−155.
(21) Ghisla, S; Massey, V. *Eur. J. Biochem.* **1989**, *181*, 1−17.
(22) Bruice, T. C. *Isr. J. Chem.* **1984**, *24*, 54−61.
(23) Mueller, F. In *Top. Curr. Chem.*; Boschke, F. L., Ed.; Springer-Verlag: Berlin, 1983; Vol. *108*, pp 71−108.
(24) Niemz, A.; Imbriglio, J.; Rotello, V. M. *J. Am. Chem. Soc.* **1997**, *119*, 887−892.
(25) Janik, B.; Elving, P. J. *Chem. Rev.* **1968**, *68*, 295−319.
(26) Michaelis, L.; Schwarzenbach, G. *J. Biol. Chem.* **1938**, *123*, 527−542.
(27) Draper, R. D.; Ingaham, L. L. *Arch. Biochem. Biophys.* **1968**, *125*, 802−808.
(28) Hartley, A. M.; Wilson, G. S. *Anal. Chem.* **1966**, *38*, 681−687.
(29) Lowe, H. J.; Clark, W. M. *J. Biol. Chem.* **1956**, *220*, 983−992.
(30) Wei, H.; Omanovic, S. *Chem. Biodiversity* **2008**, *5*, 1622−1639.
(31) Cable, M.; Smith, E. T. *Anal. Chim. Acta* **2005**, *537*, 299−306.
(32) Ksenzhek, O. S.; Petrova, S. A. *Bioelectrochem. Bioenerg.* **1983**, *11*, 105−127.
(33) Diculescu, V. C.; Militaru, A.; Shah, A.; Qureshi, R.; Tugulea, L.; Brett, A. M. O. *J. Electroanal. Chem.* **2010**, *647*, 1−7.
(34) Male, R.; Samotowka, M. A.; Allendoerfer, R. D. *Electroanalysis* **1989**, *1*, 333−339.
(35) Kay, C. J.; Solomonson, L. P.; Barber, M. J. *Biochemistry* **1990**, *29*, 10823−10828.
(36) Iyanagi, T. *Biochemistry* **1977**, *16*, 2725−2730.
(37) Heering, H. A.; Hagen, W. R. *J. Electroanal. Chem.* **1996**, *404*, 249−260.
(38) Paulsen, K. E.; Stankovich, M. T.; Stockman, B. J.; Markley, J. L. *Arch. Biochem. Biophys.* **1990**, *280*, 68−73.
(39) Tatwawadi, S. V.; Santhanam, K. S. V.; Bard, A. J. *J. Electroanal. Chem.* **1968**, *17*, 411−420.
(40) Sawyer, D. T.; McCreery, R. L. *Inorg. Chem.* **1972**, *11*, 779−782.
(41) Hammerich, O.; Svensmark, B. In *Organic Electrochemistry*, 3rd ed.; Lund, H., Baizer, M. M., Eds.; Marcel Dekker: New York, 1991; Chapter 16.
(42) Gupta, N.; Linschitz, H. *J. Am. Chem. Soc.* **1997**, *119*, 6384−6391.
(43) Quan, M.; Sanchez, D.; Wasylkiw, M. F.; Smith, D. K. *J. Am. Chem. Soc.* **2007**, *129*, 12847−12856.
(44) Hui, Y.; Chng, E. L. K.; Chng, C. Y. L.; Poh, H. L.; Webster, R. D. *J. Am. Chem. Soc.* **2009**, *131*, 1523−1534.
(45) Hui, Y.; Chng, E. L. K.; Chua, L. P.-L.; Liu, W. Z.; Webster, R. D. *Anal. Chem.* **2010**, *82*, 1928−1934.
(46) Amatore, C.; Savéant, J.-M. *J. Electroanal. Chem.* **1977**, *85*, 27−46.
(47) Hui, Y.; Webster, R. D. *Anal. Chem.* **2011**, *83*, 976−981.
(48) Bard, A. J.; Faulkner, L. R. *Electrochemical Methods: Fundamentals and Applications*, 2nd ed.; Wiley: New York, 2001.
(49) Bond, A. M.; Henderson, T. L. E.; Mann, D. R.; Mann, T. F.; Thormann, W.; Zoski, C. G. *Anal. Chem.* **1988**, *60*, 1878−1882.
(50) Geiger, W. E. *Prog. Inorg. Chem.* **1985**, *33*, 275−352.
(51) Evans, D. H.; O'Connell, K. M. *Electroanal. Chem.* **1986**, *14*, 113−207.
(52) Evans, D. H. *Chem. Rev.* **1990**, *90*, 739−751.
(53) Araki, K.; Shu, C.-F.; Anson, F. C. *Inorg. Chem.* **1991**, *30*, 3043−3047.
(54) Bond, A. M.; Feldberg, S. W.; Greenhill, H. B.; Mahon, P. J.; Colton, R.; Whyte, T. *Anal. Chem.* **1992**, *64*, 1014−1021.
(55) Richards, T. C.; Geiger, W. E. *J. Am. Chem. Soc.* **1994**, *116*, 2028−2033.
(56) Hecht, M.; Schultz, F. A.; Speiser, B. *Inorg. Chem.* **1996**, *35*, 5555−5563.
(57) Pierce, D. T.; Hatfield, T. L.; Billo, E. J.; Ping, Y. *Inorg. Chem.* **1997**, *36*, 2950−2955.
(58) Hong, S. H.; Evans, D. H.; Nelson, S. F.; Ismagilov, R. F. *J. Electroanal. Chem.* **2000**, *486*, 75−84.
(59) Batchelor, R. J.; Einstein, F. W. B.; Gay, I. D.; Gu, J.-H.; Mehta, S.; Pinto, B. M.; Zhou, X.-M. *Inorg. Chem.* **2000**, *39*, 2558−2571.
(60) Galijasevic, S.; Krylova, K.; Koenigbauer, M. J.; Jaeger, G. S.; Bushendorf, J. D.; Heeg, M. J.; Ochrymowycz, L. A.; Taschner, M. J.; Rorabacher, D. B. *J. Chem. Soc., Dalton Trans.* **2003**, 1577−1586.
(61) Shaw, M. J.; Hyde, J.; White, C.; Geiger, W. E. *Organometallics* **2004**, *23*, 2205−2208.
(62) Kuan, S. L.; Leong, W. K.; Goh, L. Y.; Webster, R. D. *Organometallics* **2005**, *24*, 4639−4648.
(63) Hong, S. H.; Evans, D. H.; Nelsen, S. F.; Ismagilov, R. F. *J. Electroanal. Chem.* **2000**, *486*, 75−84.
(64) Rudolph, M.; Reddy, D. P.; Feldberg, S. W. *Anal. Chem.* **1994**, *66*, 589A−600A.
(65) Gritzner, G.; Kuta, J. *Pure Appl. Chem.* **1984**, *56*, 461−466.
(66) Connelly, N. G.; Geiger, W. E. *Chem. Rev.* **1996**, *96*, 877−910.
(67) Chang, J. P.; Fung, E. Y.; Curtis, J. C. *Inorg. Chem.* **1986**, *25*, 4233−4241.
(68) Nishida, H.; Inaka, K.; Yamanaka, M.; Kaida, S.; Kobayashi, K.; Miki, K. *Biochemistry* **1995**, *34*, 2763−2767.
(69) Iyanagi, T. *Biochemistry* **1977**, *16*, 2725−2730.
(70) Stockman, B. J.; Westler, W. M.; Mooberry, E. S.; Markley, J. L. *Biochemistry* **1988**, *27*, 136−142.

(71) Burkhart, B. M.; Ramakrishnan, B.; Yan, H.; Reedstorm, R. J.; Markley, J. L.; Straus, N. A.; Sundaralingam, M. *Acta Crystallogr., Sect. D* **1995**, *51*, 318−330.
(72) Paulsen, K. E.; Stankovich, M. T.; Stockman, B. J.; Markley, J. L. *Arch. Biochem. Biophys.* **1990**, *280*, 68−73.
(73) Barquera, B.; Morgan, J. E.; Lukoyanov, D.; Scholes, C. P.; Gennis, R. B.; Nilges, M. J. *J. Am. Chem. Soc.* **2003**, *125*, 265−275.
(74) Barquera., B.; Ramirez-Silva, L.; Morgan, J. E.; Nilges, M. J. *J. Biol. Chem.* **2006**, *281*, 36482−36491.